Reaction Path Analysis of CO_2 Reduction to Methanol through Multisite Microkinetic Modelling over $Cu/ZnO/Al_2O_3$ Catalysts

Supporting information

Anže Prašnikar[1], Damjan Lašič Jurković[1], Blaž Likozar[1]

[1] *Department of Catalysis and Chemical Reaction Engineering, National Institute of Chemistry, Hajdrihova 19, 1001 Ljubljana, Slovenia*

S1. Catalytic reaction condition screening of CuZnAl sample aged at 260°C at thermodynamic equilibrium (sample R9)

Table S1: Catalytic conditions of CuZnAl sample aged at 260 °C and tested in packed bed reactor. The second part of this Table is on the next page.

Inlet							Outlet							Equlibrium Gaseq
T [°C]	p [bar]	ϕ [mL/min/g][1]	x(H2) [%]	x(CO2) [%]	x(CO) [%]	x(N2) [%]	x(H2) [%]	x(CO2) [%]	x(CO) [%]	x(H2O) [%]	x(CH3OH) [%]	x(N2) [%]	CO2 conv.[%]	CO2 conv.[%]
260	54.8	14.3	68.5	22.8	0	8.7	63.9	19	2.6696	4.8027	2.1331	8.6	20.2	25.2
240	54.8	13.7	68.5	22.8	0	8.7	65.3	20.3	1.5234	3.2638	1.7405	8.5	14.1	27.3
220	54.8	13.2	68.5	22.8	0	8.7	66.7	21.5	0.5432	1.8544	1.3112	8.5	8.2	31.1
200	54.8	12.7	68.5	22.8	0	8.7	67.5	22.1	0.1505	1.0544	0.9039	8.4	4.8	36.3
180	54.8	12.1	68.5	22.8	0	8.7	68.2	22.5	0.0331	0.5455	0.5124	8.3	2.3	42.6
160	54.8	11.6	68.5	22.8	0	8.7	68.4	22.6	0.0053	0.232	0.2268	8.6	1.3	49.9
260	56.4	13.8	59.1	29.5	0	11.4	54.6	26	2.7951	4.5146	1.7195	11.3	14.9	19.5
240	56.4	13.3	59.1	29.5	0	11.4	56.1	27.5	1.361	2.7955	1.4344	11.3	9.5	20.7
220	56.4	12.8	59.1	29.5	0	11.4	57.4	28.6	0.4612	1.5603	1.099	11.2	5.2	23.2
200	56.4	12.3	59.1	29.5	0	11.4	58.2	29	0.1278	0.8725	0.7446	11.2	3.2	26.9
180	56.4	11.8	59.1	29.5	0	11.4	58.7	29.3	0.0278	0.4374	0.4096	11.1	1.5	31.5
260	53.8	14.5	74.4	18.5	0	7.1	69	14.7	2.3763	4.7349	2.3586	7.1	24.3	29.9
240	53.8	14	74.4	18.5	0	7.1	71	15.7	1.5799	3.4919	1.912	6.9	18.4	32.8
220	53.8	13.4	74.4	18.5	0	7.1	72.4	17	0.6237	2.0388	1.4151	6.8	10.7	37.5
200	53.8	12.9	74.4	18.5	0	7.1	73.3	17.7	0.1825	1.167	0.9845	6.7	6.2	43.8
180	53.8	12.3	74.4	18.5	0	7.1	74	18.1	0.0416	0.632	0.5904	6.7	3.3	51.2

[1] at reaction conditions

Continuing Table S2: Catalytic conditions of CZA sample aged at 260 °C and tested in packed bed reactor.

Inlet							Outlet							Equlibrium Gaseq
T [°C]	p [bar]	ϕ [mL/min/g]	x(H2) [%]	x(CO2) [%]	x(CO) [%]	x(N2) [%]	x(H2) [%]	x(CO2) [%]	x(CO) [%]	x(H2O) [%]	x(CH3OH) [%]	x(N2) [%]	CO2 conv.[%]	CO2 conv.[%]
260	53.2	14.7	78.4	15.7	0	6	74.9	12	2.0016	4.4557	2.454	5.5	27.3	33.8
240	53.2	14.1	78.4	15.7	0	6	75.6	13	1.3524	3.2873	1.9349	5.6	20.4	37.3
220	53.2	13.6	78.4	15.7	0	6	76.8	14.2	0.5343	1.94	1.4056	5.6	12.1	42.6
200	53.2	13	78.4	15.7	0	6	77.6	14.9	0.1565	1.105	0.9485	5.6	6.9	49.6
180	53.2	12.5	78.4	15.7	0	6	78.2	15.2	0.0351	0.5989	0.5639	5.5	4.3	57.7
260	53.7	14.5	68.3	18.4	6.4	6.9	64.7	18	5.6309	1.2925	2.4423	7.4	7.0	17.4
240	53.7	14	68.3	18.4	6.4	6.9	65.3	16.4	7.6347	2.6268	1.6637	6.8	13.8	20.0
220	53.7	13.5	68.3	18.4	6.4	6.9	66.5	17.2	7.1195	1.5703	1.037	6.8	8.5	24.4
200	53.7	12.9	68.3	18.4	6.4	6.9	67.1	17.5	7.0215	1.1116	0.6207	6.7	6.1	30.4
180	53.7	12.4	68.3	18.4	6.4	6.9	67.6	17.7	6.9832	0.8158	0.3243	6.7	4.4	37.7
260	54.8	7.1	68.5	22.8	0	8.7	63	18.7	2.6248	5.435	2.8101	8.7	22.6	25.8
240	54.8	6.9	68.5	22.8	0	8.7	64.1	19.5	2.097	4.4004	2.3034	8.6	18.4	28.0
220	54.8	6.6	68.5	22.8	0	8.7	65.7	20.9	0.9872	2.7418	1.7546	8.5	11.6	31.8
200	54.8	6.3	68.5	22.8	0	8.7	66.9	21.8	0.3063	1.5735	1.2671	8.4	6.8	36.9
180	54.8	6.1	68.5	22.8	0	8.7	67.8	22.3	0.0721	0.8355	0.7633	8.4	3.7	43.3
160	54.8	5.8	68.5	22.8	0	8.7	68.4	22.6	0.0155	0.3818	0.3663	8.3	1.6	50.5
260	56.4	6.9	59.1	29.5	0	11.4	53.4	25.5	3.1031	5.3179	2.2148	11.4	17.4	19.5
240	56.4	6.7	59.1	29.5	0	11.4	54.8	26.7	2.0792	3.9368	1.8576	11.4	12.9	20.7
220	56.4	6.4	59.1	29.5	0	11.4	56.4	28	0.8493	2.3112	1.4619	11.3	7.9	23.2
200	56.4	6.1	59.1	29.5	0	11.4	57.5	28.8	0.2541	1.3005	1.0464	11.2	4.4	26.9
180	56.4	5.9	59.1	29.5	0	11.4	58.3	29.2	0.0615	0.6733	0.6118	11.2	2.2	31.5
260	53.8	7.3	74.4	18.5	0	7.1	69.6	14.5	2.2086	5.1846	2.9761	7	26.3	29.9
240	53.8	7	74.4	18.5	0	7.1	70.4	15.1	1.9111	4.3676	2.4564	6.9	22.4	32.8
220	53.8	6.7	74.4	18.5	0	7.1	71.8	16.4	1.0114	2.8484	1.8369	6.8	14.6	37.5
200	53.8	6.4	74.4	18.5	0	7.1	73	17.4	0.3278	1.6397	1.3119	6.7	8.4	43.8
180	53.8	6.2	74.4	18.5	0	7.1	73.7	17.9	0.085	0.9196	0.8346	6.7	4.9	51.2
260	53.2	7.3	78.4	15.7	0	6	74.9	11.9	1.8978	4.7083	2.8105	5.9	28.5	33.8
240	53.2	7.1	78.4	15.7	0	6	75.1	12.3	1.7179	4.1955	2.4776	5.8	25.5	37.3
220	53.2	6.8	78.4	15.7	0	6	76	13.4	1.0367	2.927	1.8903	5.7	17.9	42.6
200	53.2	6.5	78.4	15.7	0	6	77.1	14.4	0.3551	1.7065	1.3514	5.6	10.8	49.6
180	53.2	6.2	78.4	15.7	0	6	77.8	15	0.0913	0.9676	0.8764	5.5	6.1	57.7
260	53.7	7.3	68.3	18.4	6.4	6.9	63.2	16.9	5.8827	3.3163	4.5249	7.1	16.5	17.4
240	53.7	7	68.3	18.4	6.4	6.9	64.8	17.2	6.272	2.3015	2.8721	7	11.9	20.0
220	53.7	6.7	68.3	18.4	6.4	6.9	66.1	17.4	6.6222	1.62	1.6704	6.9	8.6	24.4
200	53.7	6.5	68.3	18.4	6.4	6.9	66.9	17.7	6.6636	1.094	1.0135	6.8	5.8	30.4
180	53.7	6.2	68.3	18.4	6.4	6.9	67.5	17.9	6.6184	0.6659	0.5716	6.7	3.8	37.7
200	54.9	105.2	68.5	22.8	0	8.7	68.2	22.6	0.0122	0.2513	0.2391	8.5	1.4	36.3
180	54.9	100.8	68.5	22.8	0	8.7	68.3	22.7	0.0021	0.1016	0.0995	8.5	0.6	42.7
160	54.8	96.5	68.5	22.8	0	8.7	68.5	22.8	0	0.0364	0.0364	8.5	0.1	49.9
140	54.8	92	68.5	22.8	0	8.7	68.5	22.8	0	0.01	0.01	8.5	0.0	57.6
120	54.8	87.6	68.5	22.8	0	8.7	68.5	22.8	0	0.0017	0.0017	8.5	0.0	65.5

S2.Reaction rate coefficients

Our study and selection of the active site structure is based on the landmark study by Fujitani et al.[1] where they used surface technique (XPS-X-ray photoelectron spectrocopy) to determine the reaction intermediates on Zn/Cu(111) model catalyst. They observed linear coverage increase with increasing Zn coverage of O and C species in the ratio of O/C=2 asigned to HCOO species. Difference between O in HCOO or O in ZnO was observed due to different binding energy of O 1s XPS spectra. The binding energy of Zn 2p3/2 slightly increased after being exposed to reaction condition in comparison to the reduced sample, showing oxidation of Zn species by formate groups at Zn coverage below 0.3. In fact, the binding energy of Zn 2p3/2 increased when increasing Zn coverage over 0.19 revieling difference in Zn oxidation, between ZnO and Zn-HCOO in favor of milder oxidation in the case of Zn-HCOO. This is very strong evidence that the active Zn on Cu surface during reaction is not oxidized in the same extent as ZnO. In addition, nonsimetrical formate species were also identified by in-situ infrared reflection absorption spectroscopy (IRAS) relating to adsorption of formate on neighbouring Cu and Zn atoms.[2]

The difference between XPS studies by Kattel et al.[3] (observed ZnO after reaction) and Fujitani et al.[1] (observed Zn-HCOO) is in the fact that reaction intermediates coverage decrease in the absence of H2 and CO2 by decomposition, leaving catalyst surface without carbon containing intermediates and evidently fully oxidized Zn. To reiterate, in the study by Kattel et al. they cooled the surface in the absence of H2 in CO2 while in the study by Fujitani et al. they left flow of H2 and CO2 during coolling and therefore observed HCOO on the catalyst surface.

DFT model development

Original constants of Zn/Cu(211) model structure were calculated by Kattel et al.[3] by using the density functional theory (DFT) with Vienna ab-initio simulation package code (VASP)[4] which is one of the most used DFT routines.[5–8]. For more information about DFT model explanation the reader is referred to the original source.[3] To summarize from the paper, the generalized gradient approximation PW91 (of Perdew and Wang) was used, which is not completely equivalent to PBE [9], but is still used with satisfactory results in many applications.[10,11] PAW pseudopotentials[9] with a kinetic cut-off energy of 400 eV were used which is higher than in similar computation study[12]. Additionally, to obtain faster convergence, Gaussian smearing methods with k_bT=0.05 eV were used. A 3 × 3 × 1 Monkhorst-Pack [13] grid and gamma point special k-points was used for Brillouin-zone integration. The climbing image nudged elastic band (CI-NEB) method (43) was used to obtain the location of the chemical reaction.[14]

Table S1: Optimized reaction rate coefficients for Arrhenius relation. "&" represents Cu sites and "*" represents Zn sites. If not directly specified, the original values are obtained from [3].

	optimized				original Zn/Cu(211)			
Reaction	A_{for} [s^{-1}]	Ea_{for} [kJ/mol]	A_{back} [s^{-1}]	Ea_{back} [kJ/mol]	A_{for} [s^{-1}]	Ea_{for} [kJ/mol]	A_{back} [s^{-1}]	Ea_{back} [kJ/mol]
H2 + & + & ⇌ H& + H&	1.00E+03 [e]	51.00	1.77E+12	78.00	1.00E+03 [d e]	51.00 [d]	1.77E+12 [d]	78.00 [d]
H& + CO2* ⇌ HOCO*&	4.62E+13	83.80	8.23E+13	104.28	3.91E+12	95.53	1.00E+11 [c]	123.51
H& + H2CO*& ⇌ H3CO*& + &	3.12E+08	8.47	1.17E+11	88.29	4.66E+12	11.58	1.00E+11 [c]	114.82
H& + H3CO*& ⇌ CH3OH*& + &	3.28E+12	112.01	6.98E+12	87.02	1.99E+14	143.77	1.44E+13	116.75
H& + CO2* ⇌ HCOO*&	1.69E+11	58.96	5.97E+14	142.86	3.57E+12	74.30	1.00E+11 [c]	188.16
H& + HCOO*& ⇌ HCOOH*& + &	4.69E+09	60.20	2.71E+10	75.73	7.93E+12	114.82	1.77E+11	48.25
H& + HCOOH*& ⇌ H2COOH*& + &	1.13E+12	87.74	6.71E+13	75.98	1.26E+12	58.86	9.57E+13	58.86
H2COOH*& + * ⇌ H2CO*& + OH*	1.82E+13	59.21	4.26E+11	17.08	2.53E+13	50.17	1.86E+11	16.40
H& + OH* ⇌ H2O*+ &	6.43E+09	72.66	2.89E+10	72.73	1.22E+13	77.19	4.83E+11	70.44
CO2* + & ⇌ CO& + O*	3.98E+12	46.16	1.57E+12	52.88	1.04E+13	76.23	8.40E+12	65.61
H& + O* ⇌ OH*+&	5.90E+12	309.13	5.05E+10	226.11	1.88E+13	116.75	1.00E+11 [c]	198.77
HOCO*& ⇌ CO& + OH*	3.16E+10	27.99	4.89E+11	65.23	6.60E+13	22.19	1.00E+11 [c]	58.86
CO2 + * ⇌ CO2*	7.53E+02 [e]	-2.29	2.9E+09	-29.13	7.41E+02 [a e]	-2.01 [a]	1.00E+13 [b]	-30.88
CH3OH + * + & ⇌ CH3OH*&	2.59E+01 [e]	-0.99	1.34E+13	43.01	8.68E+02 [a e]	-2.01 [a]	1.00E+13 [b]	39.56
H2O + * ⇌ H2O*	8.38E+02 [e]	-1.69	1.31E+12	39.45	1.16E+03 [a e]	-2.01 [a]	1.00E+13 [b]	37.63
CO + & ⇌ CO&	2.86E+02 [e]	-0.98	3.25E+13	59.12	9.28E+02 [a e]	-2.01 [a]	1.00E+13 [b]	98.42

[a] Collision theory

[b] Obtained from [15]

[c] Value not available in [3]. Initial value set near to the lowest A_{back} 10^{11} and allowed to be optimized.

[d] Obtained from [16] and not optimized

[e] Units are [$Pa^{-1}s^{-1}$]

S3. Detailed description of composition-activity relations determination

Relevant information about the TOF ratio determination can be found in Table S2.

Table S2: Additional information on TOF ratio determination.

Source		Van den Berg [17]	Fujitani et al.[18]	Günther et al. [19]	Fujitani et al. [20]	Kurtz et al. [21]	Saito et al. [22]	Schuman et al.[23]	Behrens et al.[24]
TOF ratio [/]	CuZn/CuSi	10	16-27	>10	4	-	8.1	-	-
	CuZnAl/CuSi	-	-	-	3.4-4.5	-	-	-	-
	CuAl/CuSi	-	-	-	2.7	-	3	-	-
	CuZnAl/CuAl	-	-	-	1.3-1.6	1.9-2.8	2.7	-	-
	CuZn/CuAl	-	-	-	1.5	1.5-1.7	-	1.3	0.95
T(reaction) [°C]		260	250	220	250	200	250	230	210
WHSV [$cm^3/g/h$]		[a]	18000	[b]	18000	30000	[c]	120000	[h]
T(reduction) [°C]		250	250	250	250	240	300	250	250
t(reduction) [h]		2.5	-	2	-	2	2	1.5	0.5
p(H_2) reduction [bar]		0.2	5	0.05	5	0.021	0.1	0.2	0.05
d(Zn) [nm]		[d]	[d]	10-21	[d]	[d]	[e]	9.5-12.5 (XRD)	5-10 (TEM)
p(H_2) [bar]		24	37.5	0.72	37.5	0.72	37.5	17.7	35.7
p(CO_2) [bar]		2.8	12.5	0.04	12.5	0.04	11	2.4	4.8
p(CO) [bar]		9.2	0	0.1	0	0.1	1.5	1.8	3.6
d(Cu) [nm]		> 8	15-54	>5	12-19 [f]	21-160 [f]	10-50.4 [f]	10.6-11.1[f]	10-19[f]
TRC factor [g]	Cu/CuZn	0.84	1	1.8	1	2.6	1	-	-
Copper surface area determation method		TEM	N_2O RFC[i]	N_2O RFC	N_2O RFC	N_2O RFC	N_2O RFC	N_2O RFC	N_2O RFC

[a] CO2+CO conversion below 20%

[b] kinetically controlled regime

[c] mass of the catalyst used to obtain constant total copper surface area

[d] catalyst synthesized by co-precipitation method

[e] CZA, CA prepared by coprecipitation, Cu/SiO_2 prepared by impregnation

[f] Cu particle size obtained using N_2O SA and copper loading

[g] TRC factor (TOF ratio correction factor) is calculated to normalize measured activity to 250 C. This is used due to different apparent activation energies for MeOH synthesis from CO2+H2 of CuSi (80(+-20) kj/mol[25]) and CuZn (40 (+-10) kj/mol [26]). We assume, the same Ea for CuSi and CuAl samples and the same Ea for CuZn and CuZnAl. TRC factor is calculated using equation below:

$$TRC\ factor = \left(\frac{k_{Cu}}{k_{CuZn}}\right)_{250\,°C}\left(\frac{k_{CuZn}}{k_{Cu}}\right)_{T\,reaction} = exp\left[\frac{1}{R}(Ea_{CuZn} - Ea_{Cu})(\frac{1}{523\ K} - \frac{1}{T_{reaction}})\right]$$

[h] 42% CO2 conversion to equilibrium and 6% CO conversion to equilibrium

[i] N_2O RFC-N_2O reactive frontal chromatography

Several factors significantly affect the TOF ratio measurements. The method of copper surface area determination in all but one case was N_2O RFC (N_2O reactive frontal chromatography). Using this method, we overestimate the copper surface area due to partial oxidation of Zn by N_2O and can therefore underestimate the TOF for Zn containing catalysts. In our previous work,[27] we did not find any significant difference between site concentration determined by H_2 TA (only Cu surface) and N_2O pulsed surface oxidation (Zn+Cu surface) for the catalysts reduced at 240 °C in 5% H_2, although higher reduction temperature could significantly reduce ZnO. Fichtl et al.[28] observed about 30% higher site concentration determined by N_2O RFC comparing to H_2 TA. Therefore the TOF ratio between samples with and without Zn present strictly normalized to Cu surface is lower than measured. However, Kuld et al.[29] found out that the measured oxygen vacancies come from Zn atoms which are replacing Cu atoms on Cu NPs. Zn atoms therefore represent Cu atoms before reduction. It is therefore more useful to normalize the activity by N_2O methods, taking into account also the reduced ZnO on Cu.

Flow rate at catalyst evaluation should be high enough to provide kinetically relevant information. The proximity to equilibrium of CO_2 conversion at 50 bar, GHSV 20000 1/h and 240 °C is 40% for the CZA catalyst,[27] which points to some effect of reverse reaction, as seen in other studies[17],[18],[20],[22],[24]. An increase of GHSV to 40000 1/h increases catalyst's CO_2 consumption by 37%,[27] where the proximity to CO_2 conversion equilibrium is 32%. Therefore, the TOF ratio could apparently decrease when comparing high activity catalyst with low activity catalyst due to reverse reaction in the range of 50%. However, we can identify (Figure 1 in the main text) large differences in activities of materials with different composition, providing us with sufficient information about composition activity relations.

TOF ratios are also temperature dependent, since different catalysts have different apparent activation energies. For this reason we obtained the apparent activation energies of Cu and CuZn catalysts in CO_2/H_2 mixture (in Table S2) to verify whether there is a large difference between composition-activity trends. This was performed by additional regression of relative TOFs by multiplying the TOF ratios using the TRC factor (TOF ratio correction factor). In Figure S1 we can observe only a minor increase of relative MeOH TOF for the CuAl catalyst.

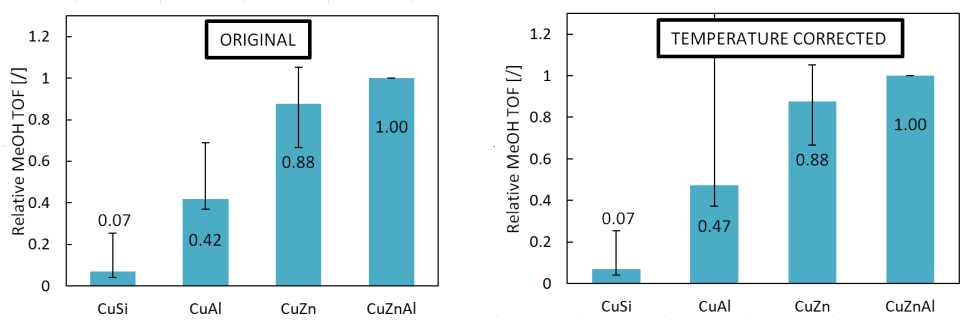

Figure S1: Relative MeOH TOF factor comparison of the original and reaction temperature corrected TOF ratios.

S4. Description of Relative MeOH TOF factor determination

The relative MeOH TOF factor was determined by using the following expression:

$$\min\left(\sum_{i=1}^{N_{TOF\,ratio}}\left(TOF\ ratio_{\frac{CuX_i}{CuY_i}}^{measured}-\frac{TOF_{CuX_i}}{TOF_{CuY_i}}\right)^2\right), X_i\ \in (\mathrm{Si, Al, Zn, ZnAl}), Y_i \in (\mathrm{Si, Al, Zn, ZnAl}) \qquad \text{(Eq. S1)}$$

Here $N_{TOF\ ratio}$ represent number of measured points and TOF_{CuXi} and TOF_{CuYi} are the variables that are optimized between 0 and 1. We used the average measured TOF ratio reported in a single study.

The errorbars are calculated by accounting deviation difference between optimized TOF ratio and measured TOF. This is presented on the case with CuZn and CuZnAl:

$$\frac{TOF_{CuZn}+\Delta TOF_{CuZn}}{TOF_{CuZnAl}+\Delta TOF_{CuZnAl}}=TOF\ ratio_{\frac{CuZn}{CuZnAl}}^{measured}$$

Since TOF ratios are the input, we cannot determine both Δ. It is also not necessarry, since we can determine the uncertainty of one catalyst in respect to the other. We therefore attribute all deviation to the less active catalyst system, therefore ΔTOF_{CuZnAl}=0. This is also reasonable, since errors are larger when using catalysts with lower activity. Therefore:

$$\Delta TOF_{CuZn}=\frac{TOF_{CuZnAl}}{TOF_{CuZn}}TOF\ ratio_{\frac{CuZn}{CuZnAl}}^{measured}$$

This is performed for all measured TOF ratios. As mentioned we account all the deviation to the catalyst system with smaller TOF. The ΔTOF_{CuAl} are therefore obtained using $ratio_{\frac{CuAl}{X}}^{measured}$, where X is CuZnAl, CuZn but not to CuSi, since for the ΔTOF_{CuSi} is determined from CuAl (and CuZnAl, CuZn).

From the list we compare deviations and select the highest positive and the lowest negative deviations and plot them on figure of Relative MeOH TOF. Of course, by this way the error bars for CuZnAl systems are 0, since all deviation is attributed to the catalysts with lower activity. The list of all TOF deviations can be found in table below.

Table 3: List of all TOF deviations. Only maximum and minimum are selected for error bar drawing.

Points	ΔTOF CuSi	ΔTOF CuAl	ΔTOF CuZn	ΔTOF CuZnAl
1	0.02	**0.27**	0.15	
2	**-0.03**	0.01	**-0.21**	
3	0.15	**-0.05**	-0.11	
4	0.04	0.17	**0.17**	
5	**0.18**	0.13		
6	0.08			
7	0.07			
max	0.18	0.27	0.17	0
min	-0.03	-0.05	-0.21	0

S5. Determination of apparent catalytic parameters for catalysts with high and low ZnO_X coverage

R3 is the CZA catalyst with 23% ZnOx coverage over Cu and R4 is the CZA catalyst with 7.1% ZnOx coverage over Cu. Figures S2 to S6 include comparison of the model and experimental data for the determination of reaction orders and kinetic constants.

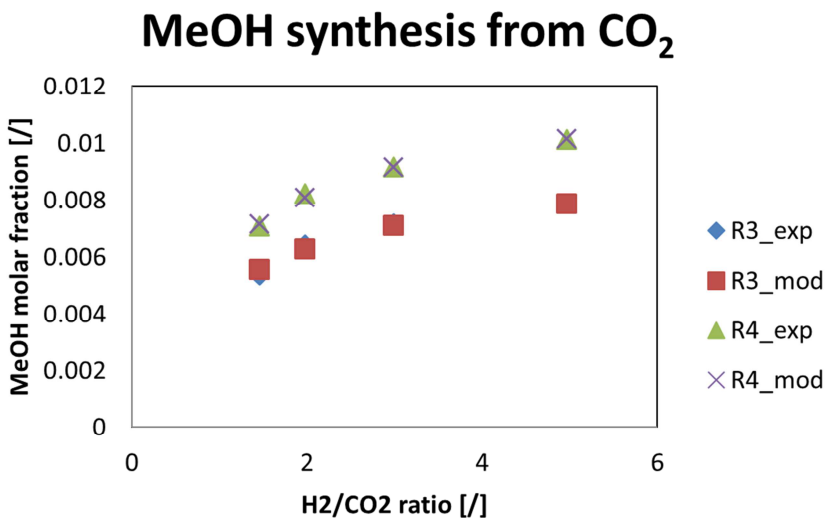

Figure S2: Comparison of model and experimental data for MeOH synthesis from CO2.

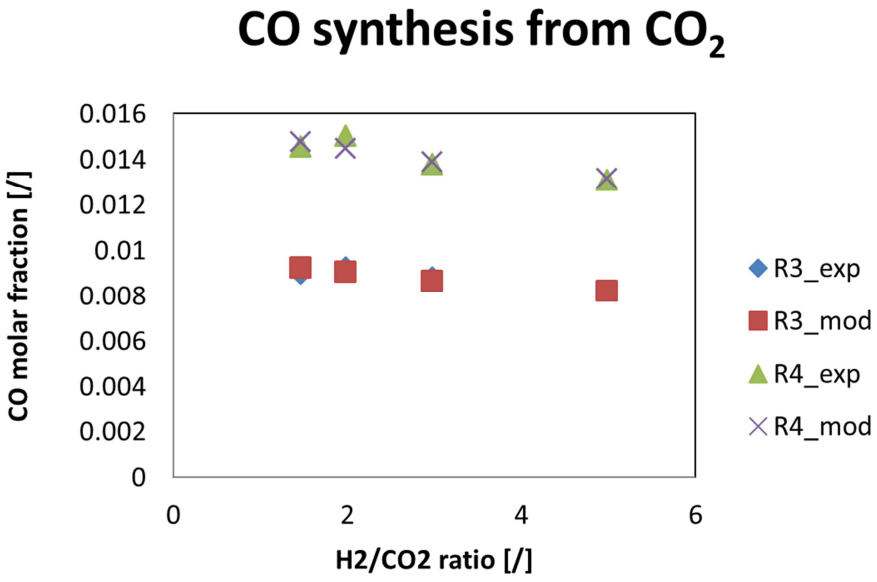

Figure S3: Comparison of model and experimental data for CO synthesis from CO2

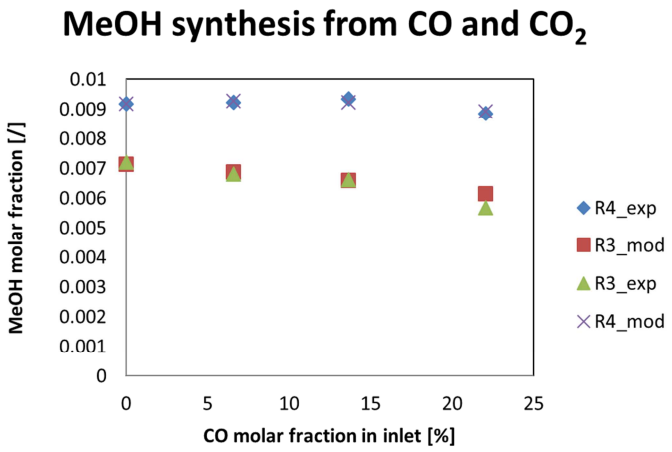

Figure S4: Comparison of model and experimental data for MeOH synthesis from CO2 and CO.

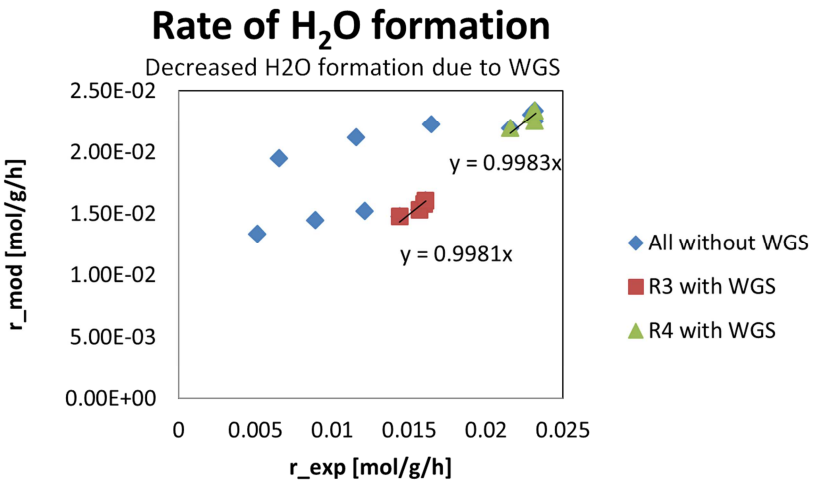

Figure S5: Comparison of model and experimental data for H2O formation with and without water gas shift reaction.

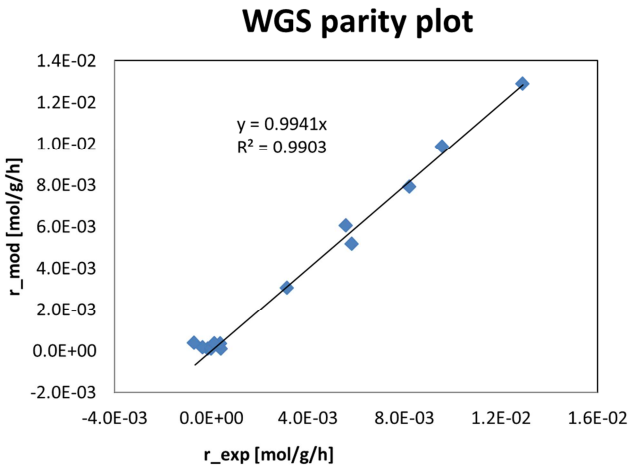

Figure S6: Comparison of model and experimental data for the rate of WGS reaction.

S6. Long-term ZnO overgrowing effect on catalytic activity

The ZnO overgrowing was also observed in our previous work in the presence of large concentration of CO and MeOH formed by CO2 hydrogenation.[27] Overgrowing was quantified by determination of calculation of exposed Cu crystallite surface fraction:

$$ECSF_{Cu}[\%] = \frac{S_{Cu}^{N_2O}}{S_{Cu}^{XRD}} 100; S_{Cu}^{XRD} = \frac{6\, L_{Cu}}{\rho_{Cu} d_{Cu}^{XRD}}, \quad \text{(Eq. S2)}$$

where S_{Cu}^{XRD} represents surface of Cu crystallites, which is calculated using copper crystallite size d_{Cu}^{XRD}, copper loading (L_{Cu}=0.277 gCu/gcat), and copper density 8.92 g/mL, assuming spherical crystallite shape.

The longest test catalytic test to our knowledge with reported XRD and N_2O chemisorption measurements on CZA catalyst were developed by Lunkenbein et al. [30] To obtain the trends of dependence on time, we fitted the surface measured by N_2O chemisorption, copper particle size and activity (Figure S7). Then we calculated the exposed copper crystallite surface fraction ($ECSF_{Cu}$) and TOF (Figure S8). The $ECSF_{Cu}$ decreased linearly after 15 days, while turnover frequency for methanol synthesis remains almost constant after 50 days. From 50 day to 148 days the $ECSF_{Cu}$ decreased by 0.08, which is 23% of the active surface and the modelled turnover frequency changed only by 2%. The initial drop of TOF could be due to agglomeration of Zn atoms after reduction. The decrease of exposed copper in this catalyst sample was also observed by electron microscopy.[30]

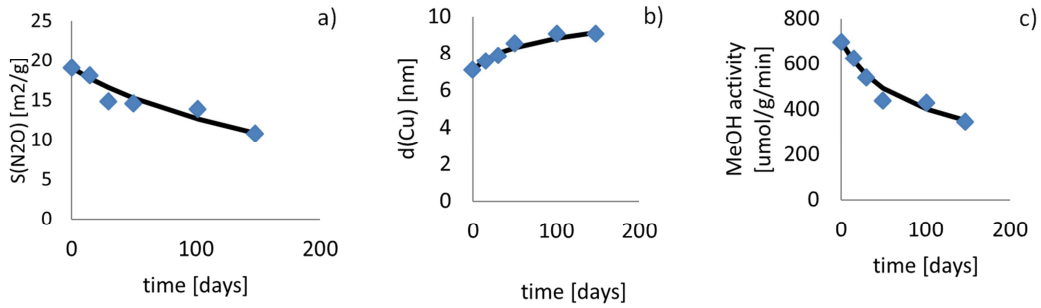

Figure S7: Model preparation for a) surface area by N2O chemisorption b) particle size determination and c) methanol activity.

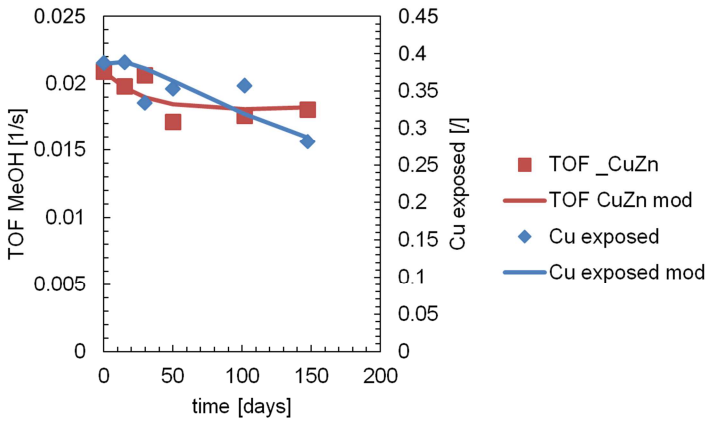

Figure S8: Effect of drop of exposed Cu surface fraction on intrinsic activity.

S7. TOF correlation with surface composition

Equation below was used to determine the effect of the change (Δ) of Zn/Cu and Al/Cu ratios from XPS and change $ZnAl_2O_4$ weight content from Rietveld refinement comparing to the sample with no aging (R8). Optimization TOF contribution factors (f) was first performed for Zn/Cu effect, than on Zn/Cu and Al/Cu effect and on the end Zn/Cu, Al/Cu and $ZnAl_2O_4$ effect. Sufficient relation is obtained when taking into all factors.

$$TOF_{MeOH} = f(Zn) * \Delta\left(\frac{Zn}{Cu}\right)_{XPS} + f(Al) * \Delta\left(\frac{Al}{Cu}\right)_{XPS} + f(ZnAl2O4) * w(ZnAl2O4 - XRD) + TOF_{ref} \quad \text{(Eq. S2)}$$

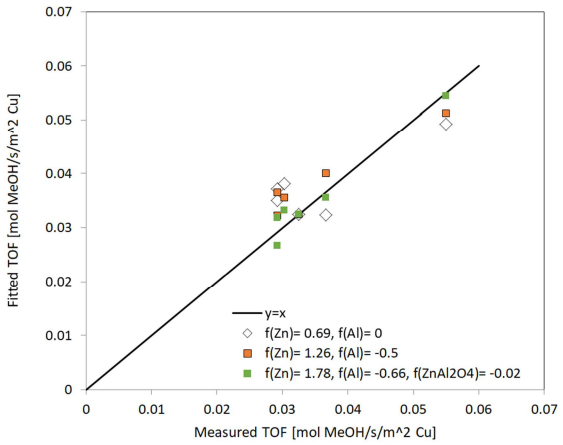

Figure S9: Parity plots of various regression minimums. Sufficient relation is obtained when taking into account Zn/Cu ratio, Al/Cu ratio and amount of spinel phase.

S8. CSTR assumption validation using PFR with axial dispersion

Peclet number is during experimental measurement equal to 1 at 50 bar and 180 °C. The mass of catalyst was varied along the flow rate variation to ensure constant Peclet number. The comparison of CSTR model and PFR model using axial dispersion was performed using axial diffusivity 1.55 10^{-6} m^2/s. We can observe from the figure below, that there is no significant change in the estimated outlet molar fractions.

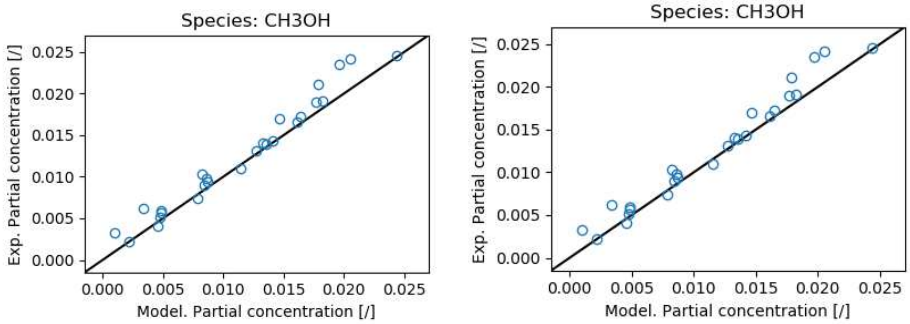

Figure S10: Left: Outlet molar fraction of MeOH using CSTR model. Right: Outlet molar fraction of MeOH using PFR+axial dispersion model.

S9. Parity plots

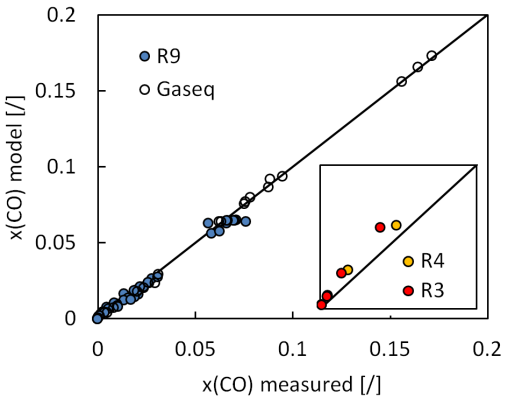

Figure S11: Parity plots of the final model for CO for all catalysts.

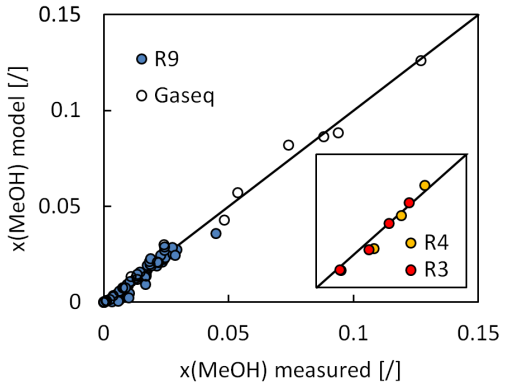

Figure S12: Parity plots of the final model for CO for all catalysts.

S10. Sensitivity analysis

Sensitivity analysis was performed on the final model at the active sites concentration of sample R9 ([Zn]=0.024 M, [Cu]= 0.0966 M) at 240 °C, 20 bar, H_2/CO_2=3, differential conditions in CSTR. The changes of MeOH and CO outlet concentrations are plotted in Figure S13 and Figure S14.

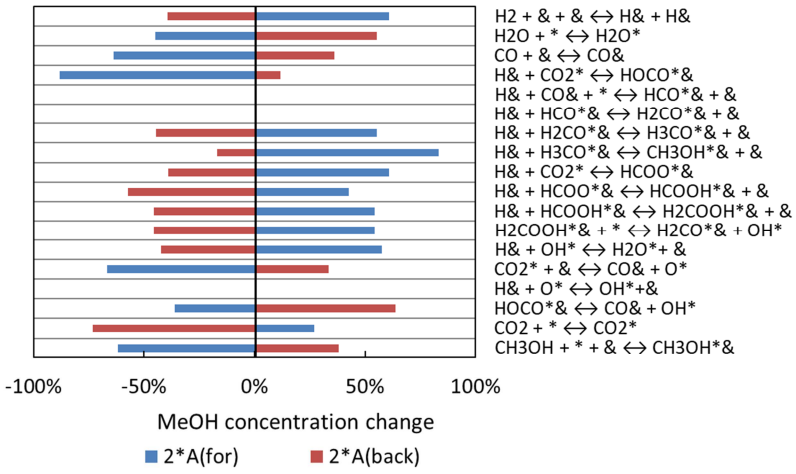

Figure S13: Change of MeOH concentration due to variation of preexponential factor variation.

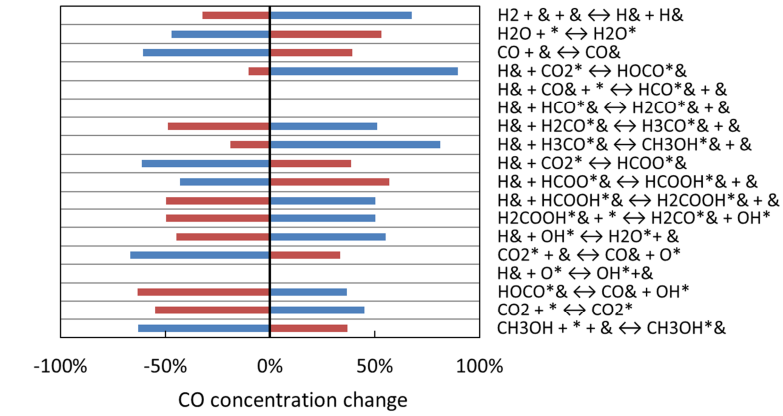

Figure S14: Change of CO concentration due to variation of preexponential factor variation.

S11. Heat and mass transfer properties

S11.1 Intra particle mass transfer limitation

Intraparticle mass transfer limitations were addressed by testing 1000 mg of fresh catalyst with particle sizes between 70 µm (fraction 40µm-100µm) and 550 µm (fraction 400µm-710 µm) at 200 °C and 250 °C, 50 bar, GHSV 15,500 h^{-1} and the ratio between H_2 and CO_2 equal to 3. We can observe in Figure S15 that the catalyst particle size does not have an influence on catalytic activity, except for the particle sizes below 100 µm, where activity dropped. This could be due to channelling effect through the catalyst bed, where preferential path of gas flow was formed, causing the decrease of overall activity. Fraction 240-400 µm was used for all other experiments.

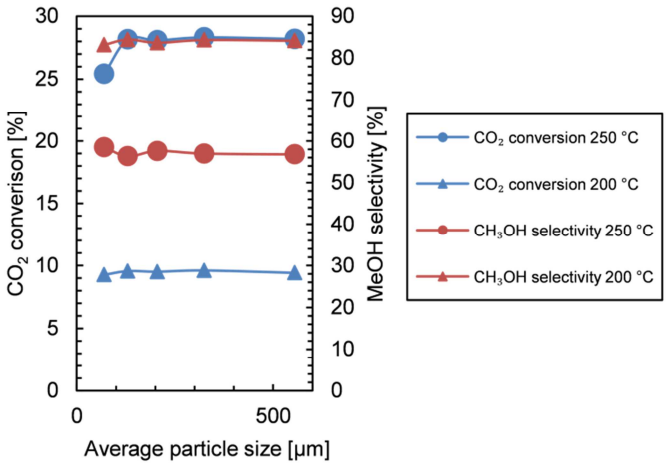

Figure S15: Catalytic test at the variation of the particle size. Conditions: 50 bar, GHSV:15,500 mL/(mL_{CAT}h), Y(H_2):Y(CO_2)=3.

S11.2 Isothermal reactor behaviour

Temperature gradient along the catalyst bed was measured by mounting additional thermocouple at the end of the catalyst bed. The bed temperature was regulated by the thermocouple immersed in the middle of the catalyst bed. Test was performed using 1000 mg of fresh catalyst at different temperatures, 50 bar, GHSV 15,500 h^{-1} and the ratio between H_2 and CO_2 equal to 3. We can observe on Figure S16 that the maximal temperature difference is below 1°C. In the combination with small reactor diameter (6.35 mm) and small temperature gradient across the bed length we can assume that the reactor is isothermal.

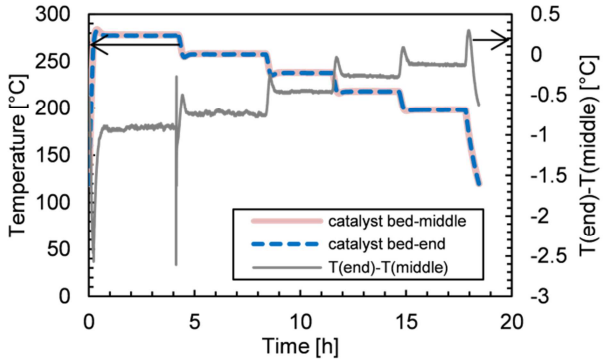

Figure S16: Temperature in the middle (red) and at the end (blue) of the catalyst bed and calculated difference (grey) between these two temperatures. The largest temperature difference at the steady state is below 1 °C. Conditions: 50 bar, GHSV:15,500 mL/(mL$_{CAT}$h), Y(H$_2$):Y(CO$_2$)=3.

S11.3 Extraparticle mass transfer limitations and axial dispersion

Catalyst mass was varied at constant GHSV to determine the impact of hydrodynamics on catalytic properties. Test was performed using fresh catalyst (240-400 µm) at 250°C , 50 bar, GHSV 15,500 h^{-1} and the ratio between H_2 and CO_2 equal to 3. We observed 10% decrease of MeOH synthesis activity when the catalyst's mass was halved, however activity could be increased by dilution in SiC to the same bed length (Figure S17). At those conditions, we therefore attribute activity decrease to axial dispersion and not to extraparticle mass transfer limitations. The reaction conditions screening (for model development) was performed at similar minimum volumetric flow as was for validation test (2 NL/h, 2.5 NL/h respectively) and at undiluted small catalyst mass (0.02-0.2 g). Due to the severe impact of axial dispersion, with Pe=1, we use CSTR model in model development and validate it using PFR+axial dispersion model.

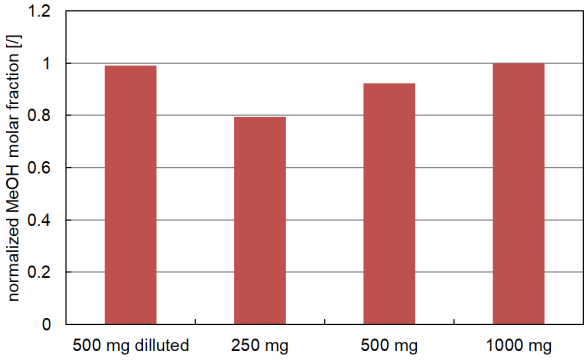

Figure S17: Catalytic test at the variation of catalyst mass at constant GHSV. Conditions: 50 bar, WHSV:12,800 mL/(g$_{CAT}$h), Y(H$_2$):Y(CO$_2$)=3. Sample "500 mg diluted" was prepared by dilution of 500 mg catalyst with SiC to the bed length equal to the sample "1000 mg".

S12. STEM-EDX

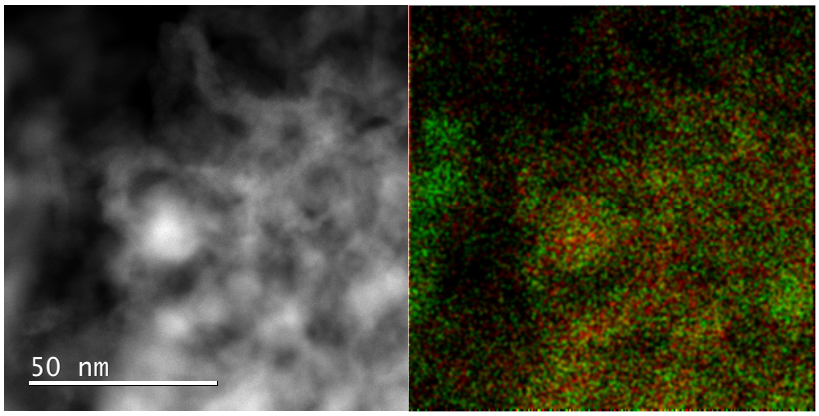

Figure S18 Left: STEM micrograph of sample reduced in H_2. Right: corresponding STEM-EDS micrograph of the same location.

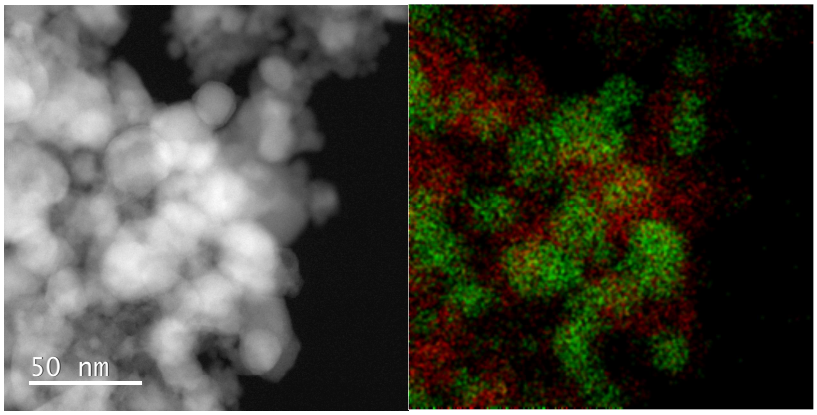

Figure S19 Left: STEM micrograph of sample reduced in H_2 and aged at equilibrium conversion of CO_2 and H_2 at 240 °C and 50 bar. Right: corresponding STEM-EDS micrograph of the same location.

S13. Additional model validation

We retrieved data from Park et al.[31] and compare molar fraction with the output molar fractions calculated using CSTR model in CERRES. The number of active sites were fitted using active Zn coverage 17.8%, where obtained Cu site concentration was 0.3 mol/L. There were no Cu surface area measurements to use it in the model definition. The comparison of CO and MeOH molar fraction can be found in Figure S20 and Figure S21. Better fit could be obtained by incorporation of plug flow reactor model with axial dispersion.

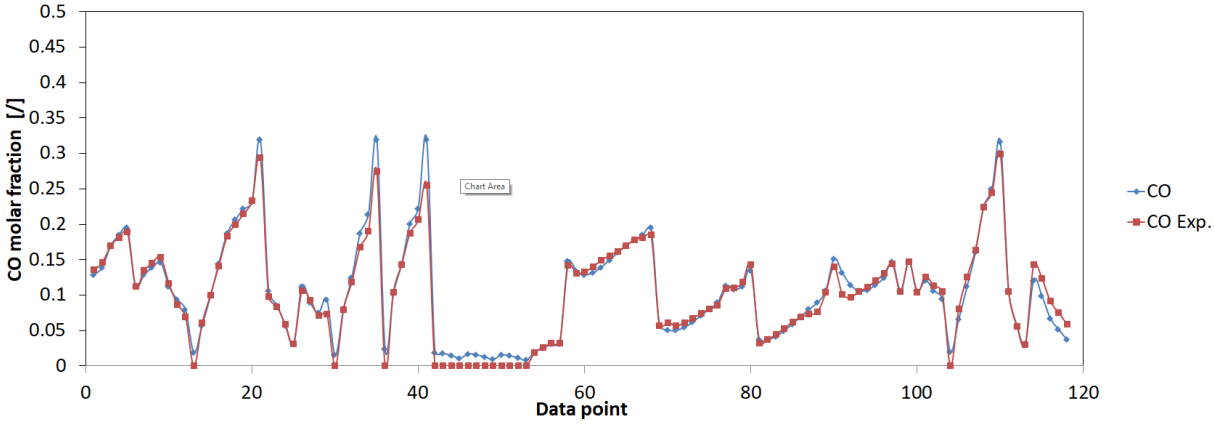

Figure S20: Comparison of CO molar fraction measured by Park et al. and calculated using our microkinetic model in CSTR mode.

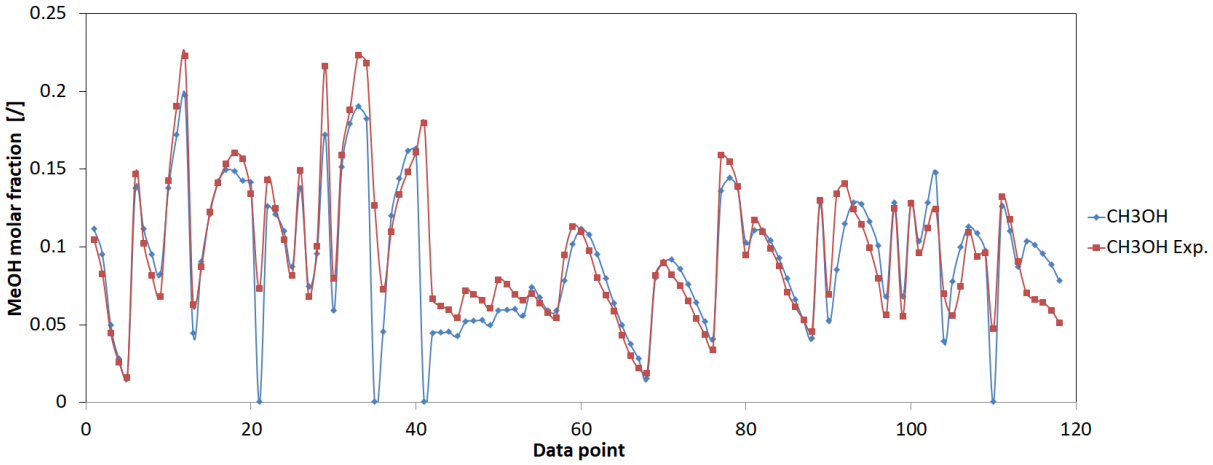

Figure S21: Comparison of MeOH molar fraction measured by Park et al. and calculated using our microkinetic model in CSTR mode. The points with 0% MeOH molar fraction, estimated using our model is due to absence of CO_2 in the gas mixture as depicted in conditions table. We assume that there was small presence of CO_2 and/or moisture, which could oxidize CO to enable MeOH formation.

S14. References

[1] T. Fujitani, I. Nakamura, T. Uchijima, The kinetics and mechanism of methanol synthesis by hydrogenation of C02 over a Zn-deposited Cu (111) surface, 383 (1997) 4–8. doi:10.1016/S0039-6028(97)00192-1.

[2] I. Nakamura, H. Nakano, T. Fujitani, T. Uchijima, J. Nakamura, Evidence for a special formate species adsorbed on the Cu – Zn active site for methanol synthesis, Surf. Sci. 404 (1998) 92–95. doi:10.1016/S0039-6028(97)00910-2.

[3] S. Kattel, P.J. Ramirez, J.G. Chen, J.A. Rodriguez, P. Liu, Active sites for CO2 hydrogenation to methanol on Cu/ZnO catalysts, Science. 355 (2017) 1296–1299. doi:10.1126/science.aal3573.

[4] G. Kresse, J. Furthmüller, Efficiency of ab-initio total energy calculations for metals and semiconductors using a plane-wave basis set, Comput. Mater. Sci. 6 (1996) 15–50. doi:10.1016/0927-0256(96)00008-0.

[5] Z.J. Zhao, A. Kulkarni, L. Vilella, J.K. Nørskov, F. Studt, Theoretical Insights into the Selective Oxidation of Methane to Methanol in Copper-Exchanged Mordenite, ACS Catal. 6 (2016) 3760–3766. doi:10.1021/acscatal.6b00440.

[6] Z. Lin, S. Lin, Y. Tian, A. Van Bokkelen, M. Valerio, M.A. Gomez, Oxygen Vacancies Altering the Trapping in the Proton Conduction Landscape of Doped Barium Zirconate, J. Phys. Chem. C. 124 (2020) 27954–27964. doi:10.1021/acs.jpcc.0c09461.

[7] A. Allouche, Software News and Updates Gabedit — A Graphical User Interface for Computational Chemistry Softwares, J. Comput. Chem. 32 (2012) 174–182. doi:10.1002/jcc.

[8] M. Huš, D. Kopač, B. Likozar, Catalytic Hydrogenation of Carbon Dioxide to Methanol: Synergistic Effect of Bifunctional Cu/Perovskite Catalysts, ACS Catal. 9 (2019) 105–116. doi:10.1021/acscatal.8b03810.

[9] A.E. Mattsson, R. Armiento, P.A. Schultz, T.R. Mattsson, Nonequivalence of the generalized gradient approximations PBE and PW91, Phys. Rev. B - Condens. Matter Mater. Phys. 73 (2006). doi:10.1103/PhysRevB.73.195123.

[10] P.L. Rodríguez-Kessler, A.R. Rodríguez-Domínguez, D. MacLeod Carey, A. Munõz-Castro, Structural characterization, reactivity, and vibrational properties of silver clusters: A new global minimum for Ag16, Phys. Chem. Chem. Phys. 22 (2020) 27255–27262. doi:10.1039/d0cp04018e.

[11] L.P. Granda-Marulanda, A. Rendón-Calle, S. Builes, F. Illas, M.T.M. Koper, F. Calle-Vallejo, A Semiempirical Method to Detect and Correct DFT-Based Gas-Phase Errors and Its Application in Electrocatalysis, ACS Catal. 10 (2020) 6900–6907. doi:10.1021/acscatal.0c01075.

[12] M. Huš, D. Kopač, N. Strah Štefančič, D. Lašič Jurković, V.D.B.C. Dasireddy, B. Likozar, Unravelling the mechanisms of CO2 hydrogenation to methanol on Cu-based catalysts using first-principles multiscale modelling and experiments, Catal. Sci. Technol. 7 (2017) 5900–5913.

doi:10.1039/c7cy01659j.

[13] J.D. Pack, H.J. Monkhorst, Special points for Brillouin-zone integrations, Phys. Rev. B. 13 (1976) 5188–5192. doi:10.1103/PhysRevB.16.1748.

[14] G. Henkelman, B.P. Uberuaga, H. Jónsson, Climbing image nudged elastic band method for finding saddle points and minimum energy paths, J. Chem. Phys. 113 (2000) 9901–9904. doi:10.1063/1.1329672.

[15] Q.-L. Tang, W.-T. Zou, R.-K. Huang, Q. Wang, X.-X. Duan, Effect of the components' interface on the synthesis of methanol over Cu/ZnO from CO2/H2 : a microkinetic analysis based on DFT + U calculations, Phys. Chem. Chem. Phys. Phys. Chem. Chem. Phys. 17 (2015) 7317–7333. doi:10.1039/c4cp05518g.

[16] H. Wilmer, O. Hinrichsen, Dynamical changes in Cu / ZnO / Al2O3 catalysts, Catal. Letters. 82 (2002) 117–122. doi:10.1023/A:1020560628950.

[17] R. van den Berg, G. Prieto, G. Korpershoek, L.I. van der Wal, A.J. van Bunningen, S. Lægsgaard-Jørgensen, P.E. de Jongh, K.P. de Jong, Structure sensitivity of Cu and CuZn catalysts relevant to industrial methanol synthesis, Nat. Commun. 7 (2016) 13057. doi:10.1038/ncomms13057.

[18] T. Fujitani, J. Nakamura, The effect of ZnO in methanol synthesis catalysts on Cu dispersion and the specific activity, Catal. Letters. 56 (1998) 119–124. doi:10.1023/A:1019000927366.

[19] M.M. Günter, T. Ressler, B. Bems, C. Büscher, T. Genger, O. Hinrichsen, M. Muhler, R. Schlögl, Implication of the microstructure of binary Cu/ZnO catalysts for their catalytic activity in methanol synthesis, Catal. Letters. 71 (2001) 37–44. doi:10.1023/A:1016696022840.

[20] T. Fujitani, M. Saito, The role of metal oxides in promoting a copper catalyst for methanol synthesis, Catal. Letters. 25 (1994) 271–276. doi:10.1007/BF00816307.

[21] M. Kurtz, H. Wilmer, T. Genger, O. Hinrichsen, M. Muhler, Deactivation of supported copper catalysts for methanol synthesis, Catal. Letters. 86 (2003) 77–80. doi:10.1023/A:1022663125977.

[22] M. Saito, J. Wu, K. Tomoda, I. Takahara, K. Murata, Effects of ZnO contained in supported Cu-based catalysts on their activities for several reactions, Catal. Letters. 83 (2002) 1–4. doi:10.1023/A:1020693226903.

[23] J. Schumann, M. Eichelbaum, T. Lunkenbein, N. Thomas, M.C. Álvarez Galván, R. Schlögl, M. Behrens, Promoting strong metal support interaction: Doping ZnO for enhanced activity of Cu/ZnO:M (M = Al, Ga, Mg) catalysts, ACS Catal. 5 (2015) 3260–3270. doi:10.1021/acscatal.5b00188.

[24] M. Behrens, S. Zander, P. Kurr, N. Jacobsen, J. Senker, G. Koch, T. Ressler, R.W. Fischer, R. Schlögl, Performance improvement of nanocatalysts by promoter-induced defects in the support material: Methanol synthesis over Cu/ZnO:Al, J. Am. Chem. Soc. 135 (2013) 6061–6068. doi:10.1021/ja310456f.

[25] A. Karelovic, G. Galdames, J.C. Medina, C. Yévenes, Y. Barra, R. Jiménez, Mechanism and structure sensitivity of methanol synthesis from CO2 over SiO2-supported Cu nanoparticles, J. Catal. 369 (2019) 415–426. doi:10.1016/j.jcat.2018.11.012.

[26] A. Karelovic, P. Ruiz, The role of copper particle size in low pressure methanol synthesis via CO2 hydrogenation over Cu/ZnO catalysts, Catal. Sci. Technol. 5 (2015) 869–881.

doi:10.1039/C4CY00848K.

[27] A. Prašnikar, A. Pavlišič, F. Ruiz-Zepeda, J. Kovač, B. Likozar, Mechanisms of Copper-Based Catalyst Deactivation during CO2 Reduction to Methanol, Ind. Eng. Chem. Res. 58 (2019) 13021–13029. doi:10.1021/acs.iecr.9b01898.

[28] M.B. Fichtl, J. Schumann, I. Kasatkin, N. Jacobsen, M. Behrens, R. Schlögl, M. Muhler, O. Hinrichsen, Counting of oxygen defects versus metal surface sites in methanol synthesis catalysts by different probe molecules, Angew. Chemie - Int. Ed. 53 (2014) 7043–7047. doi:10.1002/anie.201400575.

[29] S. Kuld, C. Conradsen, P.G. Moses, I. Chorkendorff, J. Sehested, Quantification of zinc atoms in a surface alloy on copper in an industrial-type methanol synthesis catalyst, Angew. Chemie - Int. Ed. 53 (2014) 5941–5945. doi:10.1002/anie.201311073.

[30] T. Lunkenbein, F. Girgsdies, T. Kandemir, N. Thomas, M. Behrens, R. Schlögl, E. Frei, Bridging the Time Gap: A Copper/Zinc Oxide/Aluminum Oxide Catalyst for Methanol Synthesis Studied under Industrially Relevant Conditions and Time Scales, Angew. Chemie - Int. Ed. 55 (2016) 12708–12712. doi:10.1002/anie.201603368.

[31] N. Park, M.J. Park, Y.J. Lee, K.S. Ha, K.W. Jun, Kinetic modeling of methanol synthesis over commercial catalysts based on three-site adsorption, Fuel Process. Technol. 125 (2014) 139–147. doi:10.1016/j.fuproc.2014.03.041.